Development of Wireless In-Wheel Motor Using Magnetic Resonance Coupling

Motoki Sato, *Member, IEEE*, Gaku Yamamoto, Daisuke Gunji, *Member, IEEE*, Takehiro Imura, *Member, IEEE*, and Hiroshi Fujimoto, *Senior Member, IEEE*

***Abstract*—In-wheel motors (IWMs) in electric vehicles are particularly important for motion control. A conventional IWM is powered from a battery aboard the vehicle via cables. Since power cables and signal cables of an IWM are exposed to harsh environments, they can possibly become disconnected by high acceleration or vibration. In order to overcome this problem, the wireless-in wheel motor (W-IWM) has been proposed. The risk of disconnection would disappear if the cables of the IWM are removed. One way to implement wireless power transfer is by utilizing the magnetic resonance coupling method. However, motion of the W-IWM, and thus, a misalignment between the wheel and the vehicle, leads to variations in the secondary-side voltage provided. To account for this, this paper discusses two new control methods. One proposed method maintains the secondary voltage using a hysteresis comparator. The other proposed method estimates the secondary inverter output power, applying it to a feedforward controller in order to keep the secondary dc-link voltage constant. Experimental results show that these methods can drive a W-IWM effectively with high efficiency.**

***Index Terms*—Electric vehicles (EVs), in-wheel motor (IWM), magnetic resonance coupling, wireless power transfer (WPT).**

I. Introduction

ELECTRIC vehicles (EVs) have received widespread attention in recent years for their lack of environmentally harmful emissions. Furthermore, due to the faster torque response provided by motors, EVs offer a higher degree of controllability than conventional vehicles with an internal combustion engine [1]. This is especially true with the development of individually controllable in-wheel motors (IWMs) [2], [3], which allow EVs to enjoy various control benefits such as improved comfort and an extension in electric mileage through optimal torque distribution. However, a major problem for conventional IWMs is that the power cables and signal wires from the vehicle chassis to the wheel are exposed to a harsh environment [4], [5], and may become disconnected due to continuous bending or from impact with debris from the road.

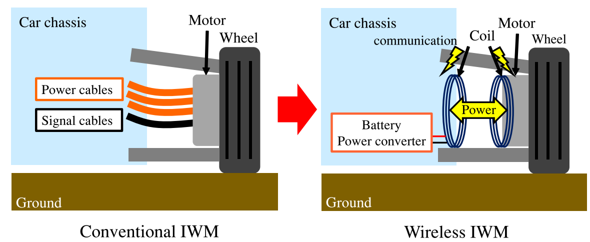

Fig. 1. Concept of the W-IWM.

To overcome this problem, an IWM that receives its power wirelessly from the vehicle chassis is proposed. This wireless in-wheel motor (W-IWM) can also be powered directly from power-transmitting coils in the road as seen in Fig. 1. Since the motor is subject to vibrations depending on the road conditions, misalignment between the motor and the vehicle can occur. Therefore, the preferred method of wireless power transfer (WPT) is magnetic resonance coupling [6], which is robust to misalignment of transmitter and receiver coils [7].

There are several different types of circuits used for WPT with magnetic resonance coupling. One type is the series-parallel (SP) circuit [8]–[10], which connects the transmitter coil and its resonant capacitors in series, while connecting the receiver coil and its resonant capacitors in parallel. With an SP circuit, a bidirectional transmitting efficiency of 90% is achieved at 2 kW [11]. However, the SP circuit requires the switching of capacitors based on the direction of power transfer, making it unsuitable for the W-IWM. On the other hand, one of the other circuit is the series–series (SS) circuit connected both the transmitter and receiver coils to resonance capacitors in series [12]–[14]. Another circuit is connected both the transmitter and receiver coils to resonance capacitors in parallel (PP) [15], [16]. Although there are no need to switch the capacitor when the regenerating, previous research on SS and PP circuits have just focused on applications to charge the battery of an EV [17]–[19], and the authors were unable to find any work involving motor control that utilized WPT.

Another major problem when powering the W-IWM is the fluctuation of the current and voltage applied to the receiving side due to the change in the alignment of the transmitter and receiver coils. In practice, the load of the W-IWM is assumed to be a permanent magnetic synchronous motor (PMSM), which is a constant power load. According to the literature, this type

Manuscript received October 16, 2014; revised April 23, 2015 and January 8, 2015; accepted September 8, 2015. Date of publication September 23, 2015; date of current version January 28, 2016. This work was supported in part by the Ministry of Education, Culture, Sports, Science, and Technology under Grant 26249061. Recommended for publication by Associate Editor C. T. Rim.

M. Sato is with the Department of Advanced Energy, The University of Tokyo, Kashiwa 277-8561, Japan, and also with the Engineering Research Division, Toyodenki Seizo, Yokohama 236-0004, Japan (e-mail: satoum@toyodenki.co.jp).

H. Fujimoto is with the Department of Advanced Energy, The University of Tokyo, Kashiwa 277-8561, Japan (e-mail: fujimoto@k.u-tokyo.ac.jp).

G. Yamamoto is with the EV System Engineering Group, Nissan Motor Co., Ltd., Atsugi 243-0123, Japan (e-mail: g-yamamoto@mail.nissan.co.jp).

T. Imura is with the Department of Electric Engineering & Information Systems, Center for Advanced Power and Environmental Technology School of Engineering, Tokyo 113-8656, Japan (e-mail: imura@hori.k.u-tokyo.ac.jp).

D. Gunji is with the Development Department 2, NSK, Ltd., Fujisawa 251-8501, Japan (e-mail: gunji@hflab.k.u-tokyo.ac.jp).

Color versions of one or more of the figures in this paper are available online at http://ieeexplore.ieee.org.

Digital Object Identifier 10.1109/TPEL.2015.2481182

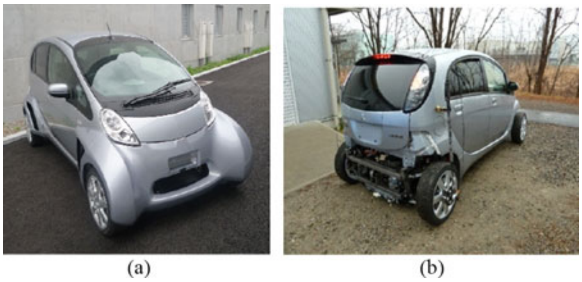

Fig. 2. Experimental vehicle FPEV4 $Sawyer$. (a) Front view. (b) Rear view.

of load will be unstable under the aforementioned conditions. Thus, it is imperative to establish a control method to drive W-IWMs that takes into account misalignment, and thus, the fluctuation of the current and voltage.

The presence of metal parts in a vehicle around the W-IWM is also a problem, as highly conductive magnetic materials near the transmitting or receiving coils can negatively affect the transmitting efficiency of the WPT via magnetic resonance coupling operated in the kilohertz to megahertz range [20]–[27]. However, the frame of the W-IWM uses iron to maintain strength of the vehicle chassis. In order to suppress the effects of these metallic materials, the placement of coils and magnetic materials must be considered when designing the system.

This paper describes the system configuration for a test unit that is to be installed in an experimental vehicle, and discusses the theory behind a method to guarantee stability in power conversion. The transmitting efficiency of the system for both powering and regenerating will also be evaluated. This paper is organized into six sections: the first section describes the introduction and background of the W-IWM. The second section shows the design concept of the W-IWM. The third section explains the outline of the W-IWM. The fourth section explains the feedback control theory of the secondary-side voltage in WPT and explains the feedforward control theory of the primary-side voltage. The fifth section shows its experimental results. The sixth section will present and analyze experimental results of the test unit. Here, primary indicates the car chassis side, and secondary indicates in-wheel side.

II. Outline of the W-IWM

A. Outline of the Experimental Vehicle

The ac electric power is transferred wirelessly via the magnetic resonance coupling method and rectified by the converter on the secondary side. The voltage is then smoothed by a filter capacitor. The control circuit for the secondary-side converters is powered by a dc/dc converter, which is also powered by power transferred from the primary side. Thus, the secondary side is able to operate without the use of any wires connecting it to the vehicle body. The authors propose a unit with maximum power equal to 6.6 kW from the two rear wheels as a primary prototype as well as the relative control and coil design for high power transmission. The capability and target specification of W-IWM is shown in Table I. The whole unit is shown in Fig. 4, where the materials, the shape, and the size of the transmitter and receiver

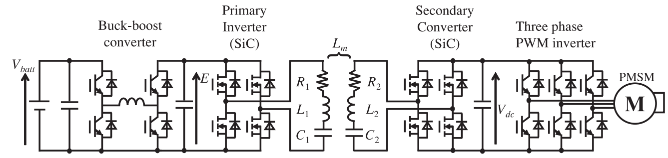

Fig. 3. Circuit of W-IWM.

Fig. 4. Structure of car chassis's unit.

TABLE I
Car Capability and the Target Specification

	Final Target	First Target
Number of IWMs	4	2
Maximum power [kW]	48	6.6
Maximum wheel torque [Nm]	1300	475

TABLE II
Coil Parameters

Parameter	Primary	Secondary
Coil resistance $R_{1,2}$	0.411 Ω	0.382 Ω
Coil inductance $L_{1,2}$	260 μH	223 μH
Capacitance $C_{1,2}$	13.5 nF	15.7 nF
Size	218 $\times$ 350 mm	218 $\times$ 300 mm
Mutual inductance L_m	48.6 μH (gap: 100 mm)	
Resonance frequency	85.0 kHz	

coils were decided according to the following considerations: In order to place the coil in the small empty space in proximity of the wheel, the coil was made planar. Eventually, the authors want to use four W-IWMs, and the gap between the two coils is set to 100 mm to account for space between the coils that would be necessary in steering the front wheels. Although several shapes of coil are considered, the possible ones are limited by the mechanical space around the W-IWM. Therefore, the author's choice is to use spiral coils that are planar.

A ferrite board on the back of both coils provides a larger mutual inductance between the coils. The use of a Litz wire reduces resistive heating and the skin effect. The parameters of the manufactured coil are reported in Table II. The resonant frequency is around 85 kHz; this value abides to the international standards of automotive wireless electricity transmission from SAE and is a main parameter in the design of the resonant capacitor [28].

Fig. 6 shows the side view of the secondary motor, and Fig. 7 shows the rear view of the secondary motor: The cover is opened.

The secondary-side circuit is mechanically and electrically embedded in the wheel. Since the full-bridge inverter on the

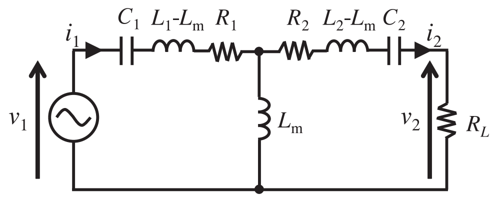

Fig. 5. Simplified equivalent circuit for WPT.

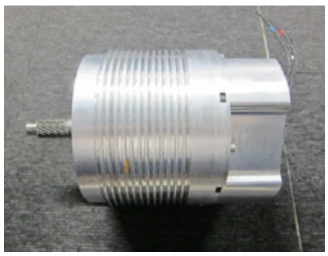

Fig. 6. Side view of the IWM.

Fig. 7. Rear view of the IWM.

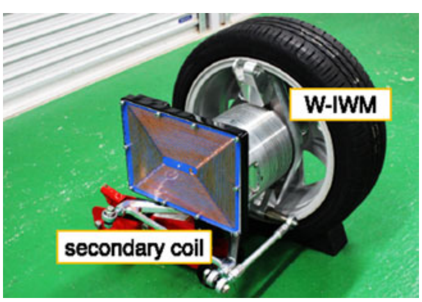

Fig. 8. Secondary-side structure (in wheel side).

secondary side operates at the high resonance frequency of the primary side, SiC MOSFETs are used in order to reduce switching losses. On the other hand, the inverter driving the motor is operated with IGBTs.

The motor output power is reduced by the reduction gear that is built in the hub bearing (the reduction ratio is 4.2), and the output power is transmitted to the wheel. The secondary-side device is shown in Fig. 8

B. Transmitter and Receiver Coil Design

Fig. 5 shows the simplified equivalent circuit of WPT. If it assumed to be fundamental power factor of secondary is unity, from the secondary rectifier to motor can be assumed genuine resistance [29]. Where, voltage amplifier ratio Av and transmitting efficiency Ap can be assessed as follows [29]:

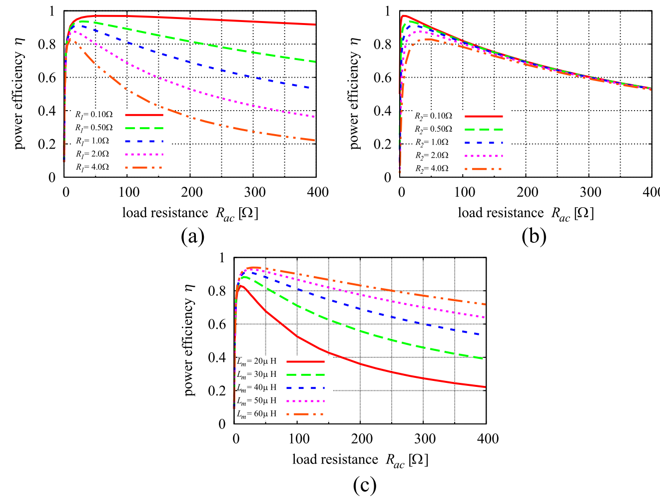

Fig. 9. Transmission efficiency versus coil parameter deviation. (a) Transmission efficiency versus $R1$ deviation. (b) Transmission efficiency versus $R2$ deviation. (c) Transmission efficiency versus Lm deviation.

$$A_V = \frac{V_2}{V_1} = j\frac{\omega_0 L_m R_{\rm ac}}{R_1 R_{\rm ac} + R_1 R_2 + (\omega_0 L_m)^2} \tag{1}$$

$$\eta = \frac{V_2 \bar{I}_2}{V_1 \bar{I}_1} = \frac{(\omega_0 L_m)^2 R_{\rm ac}}{(R_{\rm ac} + R_2)\{R_1 R_{\rm ac} + R_1 R_2 + (\omega_0 L_m)^2\}}. \tag{2}$$

The coil parameters R_1, R_2, and L_m, in (2), are coil parameters that vary based on the coil size, number of turns, and coil misalignment. Where R_1 is primary coil resistance, R_2 is secondary coil resistance, and L_m is mutual inductance. Fig. 9 shows the transmission efficiency versus coil parameter deviation. It is calculated by (2). In this study, the voltage source inverter for IWM drive at secondary side is operated by 350-V constant. The maximum output power of an IWM is 3.3 kW. According to the aforementioned conditions, equivalent resistance $R_{\rm ac}$ is calculated as follows:

$$R_{\rm ac} = \frac{V_{21}^2}{P_2}. \tag{3}$$

The relationships between V_{21} and $V_{\rm dc}$ is as follows:

$$V_{21} = \frac{2\sqrt{2}}{\pi} V_{\rm dc}. \tag{4}$$

When motor power outputs rated power, $R_{\rm ac} = 30\,\Omega$. According to (2), when $R_{\rm ac} = 30\,\Omega$, the η is almost over 90%. As a result, the coils for the W-IWM can achieve high efficiency at rated power.

Table III shows assignment values to (2).

III. Electric Power Conversion of the Transmitter and the Receiver

A. Stability Analysis of the Secondary DC-Link Voltage

The W-IWM is a PMSM driven by a voltage type inverter and is assumed to have constant dc power. In order to analyze the stability of the secondary dc-link voltage, we introduce a

TABLE III
ASSIGNMENT VALUES TO (2)

	R_1	R_2	L_m
Fig. 9(a)	0.10∼4.0 Ω	1.0 Ω	40 μH
Fig. 9(b)	1.0 Ω	0.10∼4.0 Ω	40 μH
Fig. 9(c)	1.0 Ω	1.0 Ω	20∼60 μH

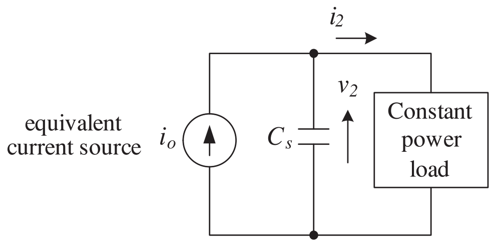

Fig. 10. Simplified circuit model.

simplified circuit model shown in Fig. 10. In this model, the primary circuit and the secondary converter are assumed to have an equivalent variable current source i_o, which is the average output current of the secondary converter. The circuit equation of the simplified model is expressed as follows:

$$i_2 = i_o - C_s \frac{dv_2}{dt}. \tag{5}$$

The load current i_2 is expressed as

$$i_2 = \frac{P_2}{v_2} \tag{6}$$

where P_2 is the load power. Substituting(6) into (5)

$$\frac{dv_2}{dt} = -\frac{P_2}{C_s v_2} + \frac{i_o}{C_s}. \tag{7}$$

Linearizing (7) around the equilibrium point

$$\begin{aligned} \frac{d\Delta v_2}{dt} &= \frac{P_2 \Delta v_2}{C_s {V_2}^2} + \frac{\Delta i_o}{C_s}. \\ v_2 &= V_2 + \Delta v_2 \\ i_o &= I_o + \Delta i_o. \end{aligned} \tag{8}$$

Transfer function $P_\Delta(s)$, which is from Δi_o to Δv_2, is derived by taking the Laplace transform of (8) as follows:

$$P_\Delta(s) = \frac{\Delta v_2(s)}{\Delta i_o(s)} = \frac{1}{C_s\left(s - \frac{P_2}{C_s {V_2}^2}\right)}. \tag{9}$$

Then, the pole of $P_\Delta(s)$, p is expressed as

$$p = \frac{P_2}{C_s {V_2}^2}. \tag{10}$$

Therefore, $P_\Delta(s)$ is unstable regardless of to the load power P_2 and the equilibrium point because $p_2 > 0$ and $V_2 > 0$. From the results of the aforementioned analysis, in the case of a constant power load, the load voltage is unstable, and stabilization control of the load voltage is necessary.

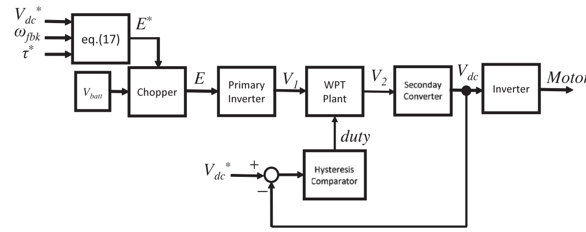

Fig. 11. Control block diagram of the W-IWM.

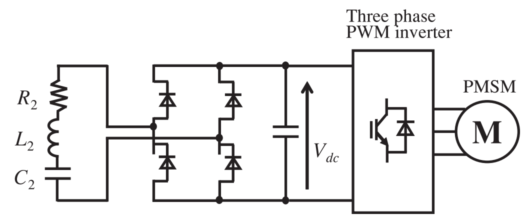

Fig. 12. Secondary circuit configuration (mode 1: diode rectifier).

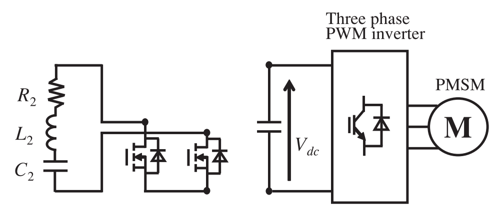

Fig. 13. Secondary circuit configuration (mode 2: short circuit).

B. Secondary DC-Link Voltage Control

Fig. 11 shows the block diagram of the W-IWM. In Fig. 11, $V_{\rm batt}$ is the voltage of the battery of the EV. $V_{\rm batt}$ is inputted into the buck–boost converter, which converts $V_{\rm batt}$ to E, the dc voltage for the primary inverter. The reference for the primary inverter voltage, E^*, is calculated from (20), which is derived from $V_{\rm dc}^*$ and τ^*, which are, respectively, dc-link torque reference for the secondary inverter and motor speed. Where the motor speed is provided to the primary side via Bluetooth communication. WPT coils means the control plant for the WPT. The secondary converter makes $V_{\rm dc}$ stable by using the hysteresis comparator. The motor is vector controlled by the secondary inverter.

Fig. 12 shows the secondary circuit configuration (mode 1: diode rectifier) as the figure that focuses on the secondary side. If the switching element on the top side is always set to OFF and the switching element on the bottom side is turned OFF, it will operate as a diode bridge rectifier circuit, and electric power will be supplied to the load. On the other hand, Fig. 13 shows the secondary circuit configuration (mode 2: short circuit). If the switching element on the bottom side is turned ON, the secondary-side coil will short circuit and the electric power will not reach the load. $V_{\rm dc}$ can be maintained near a desired value by repeating the operation mentioned above by hysteresis comparison if enough power is transferred from the primary side to the secondary side. However, if power from the primary side is insufficient,$V_{\rm dc}$ cannot be maintained at the reference voltage. The power required by the secondary side is computed from the reference torque as well as the motor speed, transmitted via

Bluetooth from the secondary side. The way to compute the primary inverter output V_1 is discussed in the next section.

C. Primary Voltage Control

The primary-side circuit unit is comprised of a bidirectional buck–boost converter and a full-bridge inverter. The switching devices used for the buck–boost converter are silicon IGBTs, while the full-bridge circuit employs SiC MOSFETs in order to reduce the switching losses that occur at 85 kHz. The system controls the voltage amplitude with the buck–boost converter, where the inverter duty ratio was fixed. The two sides communicate via Bluetooth: the motor speed is sent to the primary side, while the second sides receives the torque reference from the primary side. When $V_{\rm dc}$ on the secondary side is controlled uniformly, the secondary-side dc-link current changes according to the motors output. That is, the motor can be considered variable resistor load, which changes according to the output power. Then, the electric power needed by the secondary side is computed from the reference torque and motor speed, and feedforward control of the output voltage of a primary-side inverter is carried out based on its value. The chopper voltage reference E^* as the output of the feed-back control loop is computed as follows. The increase in voltage between coils due to WPT via magnetic resonance coupling, A_v, is expressed as [29].

$$A_v = \frac{V_2}{V_1} = \frac{\omega_0 L_m R_{\rm ac}}{R_1 R_{\rm ac} + R_1 R_2 + (\omega_0 L_m)^2} \tag{11}$$

where V_1 is the effective value of the fundamental frequency of the primary inverters output voltage, V_2 is the effective value of the fundamental frequency of the secondary converters input voltage, ω_0 is the resonant frequency of the coil, and $R_{\rm ac}$ is the equivalent resistance viewed before the secondary converter, where

$$R_{\rm ac} = \frac{8}{\pi^2} R_L \tag{12}$$

and R_L is the equivalent resistance viewed from $V_{\rm dc}$ toward the motor. However, since R_L cannot be directly measured, it is estimated as

$$R_L = \frac{\left(V_{\rm dc}{}^*\right)^2}{P_o} \tag{13}$$

where $V_{\rm dc}{}^*$ is the reference value of $V_{\rm dc}$, set to be 352.5 V. The output P_o of the secondary-side converter becomes

$$P_o = \omega_m T_{\rm ref} + M_{\rm loss} \tag{14}$$

where ω_m is the motor speed, $T_{\rm ref}$ is the reference torque, and $M_{\rm loss}$ is the copper loss of the motor. Assuming to be $T^* = T$, where T is actual torque of the W-IWM, since the system is given the rated current I_r of the W-IWM and the stator resistance R_s of the W-IWM, the $M_{\rm loss}$ is calculated to

$$M_{\rm loss} \simeq \frac{T^*}{T_{\rm rated}} {I_r}^2 R_s \tag{15}$$

where $T_{\rm rated}$ is rated torque of the W-IWM. On the other hand, because

$$V_{\rm dc} \simeq \frac{2\sqrt{2}}{\pi} V_2 \tag{16}$$

it can also be said that

$$V_1 = \frac{\pi}{2\sqrt{2}} \frac{R_1 R_2 + \frac{8}{\pi^2} R_1 R_L + {\omega_0}^2 {L_m}^2}{\frac{8}{\pi^2}\omega_0 L_m R_L} V_{\rm dc}{}^*. \tag{17}$$

ω_m is given as feedback to the primary side through Bluetooth communication. From (17) and (13), it can be said that

$$V_1 = \frac{\pi}{2\sqrt{2}} \left(\frac{R_1 R_2 + {\omega_0}^2 L_m^2}{\omega_0 L_m V_{\rm dc}{}^*} P_o + R_1 \frac{V_{\rm dc}{}^*}{\frac{8}{\pi^2}\omega_0 L_m} \right). \tag{18}$$

From the Fourier expansion of V_1 considering fundamental harmonics, (18) becomes

$$V_1 = \frac{4}{\sqrt{2}\pi} E \sin\left(\frac{\pi}{2}\right). \tag{19}$$

Therefore, the chopper reference E^*, which is assumed to be E, is expressed as

$$E^* = \frac{\pi}{4}\sqrt{2} V_1 \tag{20}$$

which, from (18), becomes

$$E^* = \frac{\pi^2}{8} \left(\frac{R_1 R_2 + {\omega_0}^2 L_m^2}{\omega_0 L_m V_{\rm dc}{}^*} P_o + R_1 \frac{V_{\rm dc}{}^*}{\frac{8}{\pi^2}\omega_0 L_m} \right). \tag{21}$$

E^* is the chopper reference, or the reference amplitude of the square-wave output voltage of the primary inverter from the chopper. However, the system has a communicative delay between the primary side and the secondary side of about 0.2 s, making the update time of the feedforward control output E^* slow. Since there is the possible case where the output power of the secondary inverter is insufficient due to the delay in Bluetooth communication, there is some offset added and E^* is multiplied by a certain gain in order compensate for any energy shortages that could be caused by the communicative delay. Of course, this delay limits the acceleration rate. If the driver knew the rate of torque reference, it is possible to feedforward the necessary amount of power instead of relying on the feedback of the wheel speed. This would not affect the acceleration of the EV, because in this case, the Bluetooth only communicates the start signal and the torque reference for the EV, which is faster than the driver reaction time.

D. Electric Power Regeneration Operation

Since the wireless electric energy conversion portion of the system is symmetric on both sides in the circuit configuration of this unit, electric power regeneration is easy. When electric power is revived from the motor and the secondary-side dc-link voltage $V_{\rm dc}$ becomes more than a threshold value, a radio signal is transmitted to the primary side from the secondary side, and control is changed so that a primary side may be operated as diode bridge rectification, while the converter on the secondary side begins operating as an inverter. The state information of regeneration is changed as follows. From the secondary inverter side

No1: If, $V_{\rm dc} < 345V$ or $V_{\rm dc} < 350$V) and $V_{\rm dc}$ is decreasing over 2 ms, the secondary inverter is shifted to powering.

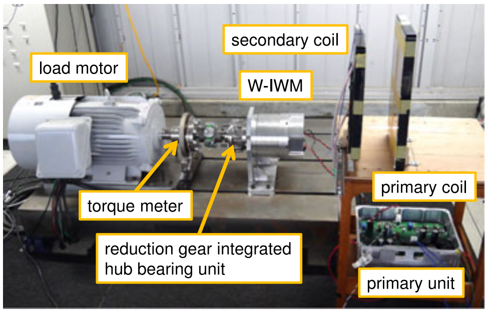

Fig. 14. Experiment set for the bench test.

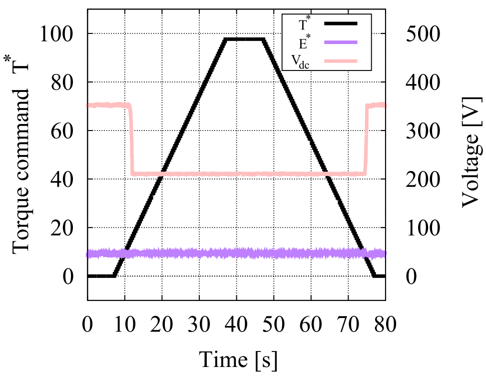

Fig. 15. V_{dc} and torque versus Time (no control).

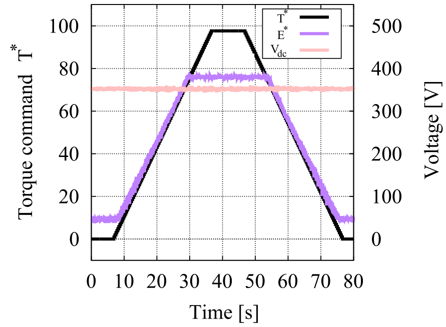

Fig. 16. V_{dc} and torque versus Time (with control).

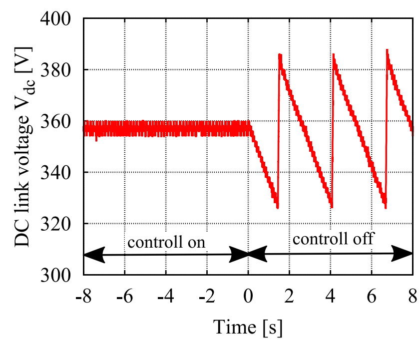

Fig. 17. V_{dc}(without secondary feedback).

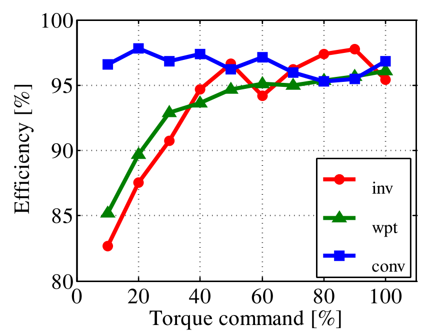

Fig. 18. Efficiency of each part of the system at 135 r/min.

No2: If, $V_{\mathrm{dc}} > 360V$ or $V_{\mathrm{dc}} < 355\ V)$ and V_{dc} is increasing over 2 ms, the secondary inverter is shifted to required to regenerating.

No3: If the secondary inverter gets the regenerating flag signal from primary inverter and the case of No2, the secondary inverter state is shifted to regenerating. Thus, the secondary converter or hysteresis comparator is changed through control to operate as a power transmitting inverter, and the primary inverter is operated as the diode rectifier.

On the primary side, when the reference of the output coil voltage is under 0 V, the regenerative flag signal is transmitted to the secondary side.

Therefore, electric power regeneration operation to the primary side from the secondary side is achieved.

IV. Experiment

A. Bench Test for W-IWM

Fig. 14 shows the experiment set for the bench test. The prototype underwent bench tests and was driven at its rated speed to examine the effectiveness of both the feedforward and feedback control methods in maintaining sufficient power on the secondary side. Fig. 15 shows the results without feedforward control. The reference torque is to change from 0% to 100%, but since the chopper reference voltage is constant, V_{dc} falls to the voltage limiter (210 V) as sufficient power is not transmitted to the secondary side. Fig. 16 shows the feedforward control result. Once again the reference torque is changed from 0% to 100%, but with the feedforward control, the chopper reference voltage, E^*, increases. This allows for the transfer of more energy to the secondary side, maintaining the secondary-side voltage, V_{dc}, at the desired voltage of 352.5 V. E^* is also shown to reach its upper limit of 380 V, but due to the secondary side being constantly provided with excess power, as discussed in Section IV-C, this does not affect the secondary side's ability to maintain a constant V_{dc}. Next, the feedback control of the secondary side based on hysteresis is evaluated. The reference value of the dc-link voltage V_{dc} is 352.5 V on the secondary side with no load, and the motor speed is 0 r/min. Fig. 17 shows the secondary-side voltage being maintained by the hysteresis comparator. Fluctuations occur, starting at 8 s, where the hysteresis width is changed to 30 V in order to demonstrate the behavior of V_{dc} without feedback control. The reference torque was changed from 0% to 100%, and the secondary-side dc-link voltage V_{dc}, where the motor maintains a rotational speed of 135 r/min, is shown in Fig. 22. Where rated motor speed is 555 r/min, the motor speed is reduced to 135 r/min by the reduction gear. Even though the reference torque has been changed, V_{dc} is controlled to be constant in the vicinity of 352.5 V. Similarly, in regeneration, the reference torque was changed from 0% to

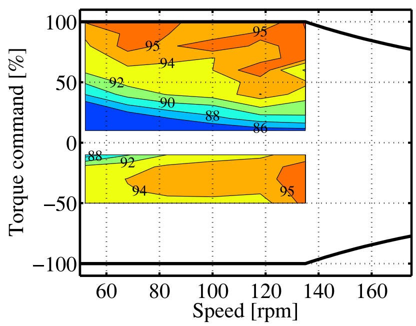

Fig. 19. Efficiency between the transmitter and receiver coils as $\eta_{\rm wpt}$.

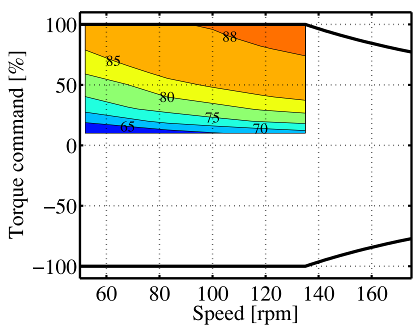

Fig. 20. Efficiency between the battery and $V_{\rm dc}$ as $\eta_{\tt total}$.

100% and the secondary-side dc-link voltage $V_{\rm dc}$, where the motor is regenerating at 67 r/min, are shown in Fig. 23.

B. Efficiency for the W-IWM

Due to the design of the prototype, the overall efficiency could not be directly measured. Similarly, measurement of the power-conversion circuit's efficiency is not possible during regeneration. Fig. 19 shows the contour of the efficiency between the transmitter and receiver coils. In Fig. 19, the efficiency of the converter when changing the reference torque while rotating at 135 r/min. Each transducer has a high efficiency of 95% when the output is large, while the power transfer efficiency between the transmitting and receiving coils, $\eta_{\rm wpt}$, and the efficiency of the primary-side inverter, $\eta_{\rm inv}$, are reduced as the output is small. The decrease of $\eta_{\rm wpt}$ is due to the characteristics of WPT, and it is an object for future improvement. In addition, the measurement results of the power at each point of the circuit, as well as the efficiency between the battery and $V_{\rm dc}$ (100% reference torque and a motor wheel speed of 135 r/min) is shown in Fig. 20. The overall efficiency of the system from the power supply to the secondary-side dc link is about 90%. This is considered to be sufficient for the application of the W-IWM in EVs. As a reference, the efficiency of each converter at the rated wheel speed of 135 r/min is shown in Fig. 18 and the efficiency at the rated power driven of each part of the W-IWM is shown in Fig. 21.

C. Influence of Misalignment

This section discusses the change in efficiency due to the misalignment of the two coils. Fig. 25 shows the relationship between transmission efficiency and the coils' misalignment, where the gap between the coils is 100 mm. Fig. 25 explains that

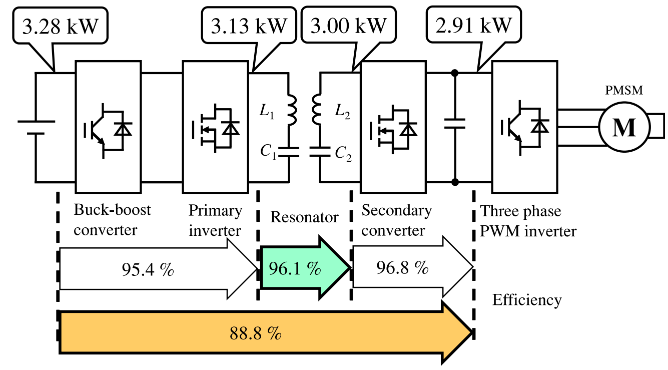

Fig. 21. Efficiency of the W-IWM at 100% torque reference.

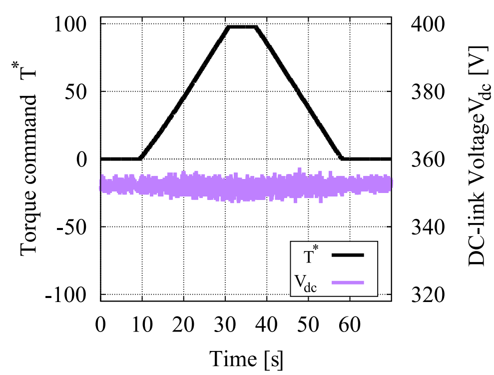

Fig. 22. Control while powering.

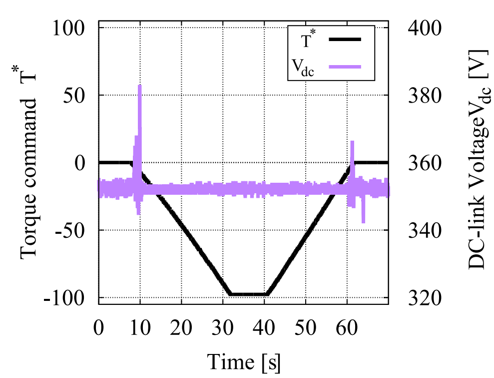

Fig. 23. Control while regenerating.

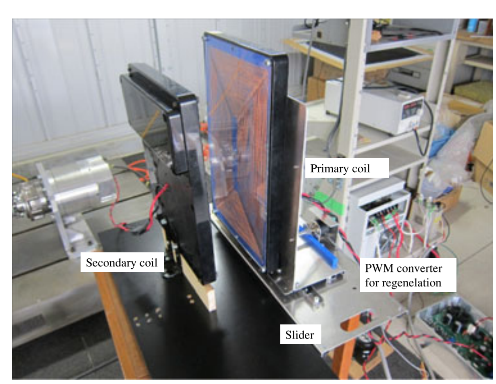

Fig. 24. Test bench setup with slider.

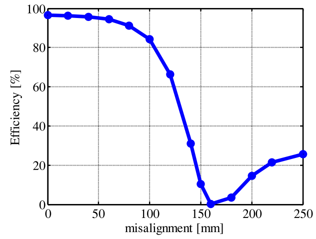

Fig. 25. Transmitting efficiency and coil misalignment.

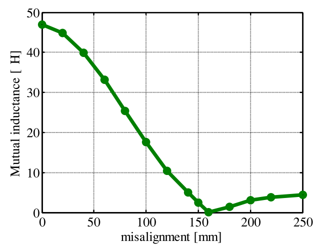

Fig. 26. Mutual inductance and coil misalignment.

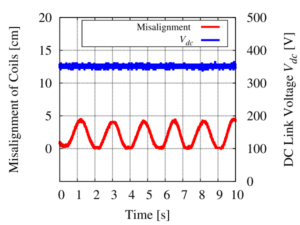

Fig. 27. Coil misalignment and dc-link voltage V_{dc} at 50% load.

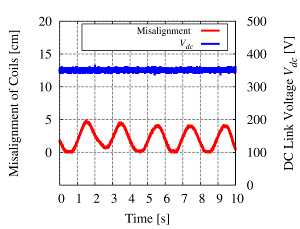

Fig. 28. Coil misalignment and dc-link voltage V_{dc} at 100% load.

there are minimal effects on efficiency when the misalignment is around 50 mm.

Fig. 26 shows the relationship between the mutual inductance of the two coils and the coils' misalignment, where the gap between the coils is100 mm. This measurement also shows that the mutual inductance has a minimal impact on the efficiency. Thus, we conclude that there is only a small decline in power for WPT.

As shown in Fig. 24, this section describes the experimental results where the motor is operated while a slider simulates the vehicle suspension vibration. The slider is fixed between the primary coil and the secondary coil. The coil misalignment that is used for the slider, is simulated by the author's hand. Fig. 27 shows the experimental results of how the coil misalignment influences the dc-link voltage, V_{dc}, at the rated wheel speed of 135 r/min and under 50% load. Fig. 28 also shows the experimental results of how coil misalignment affects V_{dc} at the rated wheel speed of 135 r/min under 100% load. Both results show that, despite the misalignment between the two coils, the dc-link voltage V_{dc} is kept stable.

V. Conclusion

In this paper, the design, implementation, and bench test results of a W-IWM were discussed. An analysis of the stability of the W-IWM as a constant power load demonstrated the need for control of the secondary-side voltage. To achieve this, a novel hysteresis control method was proposed. In addition, a feedforward control method for the primary-side voltage, based on the output of the secondary-side converter estimated from motor speed and reference torque, was also proposed. The results of the bench tests conducted on the trial unit validated the effectiveness of the proposed control methods, showing high efficiency both when powering the motor and regenerating energy. Future work will focus on the installation of a W-IWM on an EV, the analysis of its performance, and the development of road-to-vehicle wireless powering of the W-IWM.

Acknowledgements

The authors would like to thank the Murata Manufacturing Co., Ltd., for providing the laminated ceramic capacitors (U2J characteristics) used in these experiments.

References

[1] Y. Hori, "Future vehicle driven by electricity and control research on four wheel motored 'UOT electric march II'," *IEEE Trans. Ind. Electron.*, vol. 51, no. 5, pp. 954–962, Oct. 2004.

[2] S. Harada and H. Fujimoto, "Range extension control system for electric vehicles during acceleration and deceleration based on front and rear driving-braking force distribution considering slip ratio and motor loss," in *Proc. 39th Annu. Conf. IEEE Ind. Electron. Soc.*, 2013, pp. 6624–6629.

[3] S. Murata, "Vehicle dynamics innovation with in-wheel motor," presented at the JSAE EVTeC, Yokohama, Japan, 2011, Paper 20117204.

[4] NTN Corporation, WO2013108546 A1, 2013.

[5] Toyota Motor Corporation, P2012-223041A, 2012 (in Japanese).

[6] A. Kurs, A. Karalis, R. Moffatt, J. D. Joannopoulos, P. Fishe, and M. Soljacic, "Wireless power transfer via strongly coupled magnetic resonances," *Sci. Exp.*, vol. 317, no. 5834, pp. 83–86, Jun. 7, 2007.

[7] T. Imura, H. Okabe, T. Uchida, and Y. Hori, "Flexibility of contactless power transfer using magnetic resonance coupling to air gap and misalignment for EV," presented at the IEEE Electric Vehicle Driven Electric Vehicle Symp., (EVS-24), Stavanger, Norway, vol. 24, May 2009.

[8] Y. H. Chao, J. J. Shieh, C. T. Pan, and W. C. Shen, "A closed-form oriented compensator analysis for series-parallel loosely coupled inductive power transfer systems," in *Proc. Power Electron. Spec. Conf.*, 2007, pp. 1215–1220.

[9] Y. H. Chao and J. J. Shieh, "Series-parallel loosely coupled battery charger with primary-side control," in *Proc. Int. Conf. Control, Autom. Inf. Sci.*, 2012, pp. 226–230.

[10] R. Bosshard, U. Badstubner, J. W. Kolar, and I. Stevanovic, "Comparative evaluation of control methods for inductive power transfer," in *Proc. Int. Conf. Renewable Energy Res. Appl.*, 2012, pp. 1–6.

[11] S. Nakadachi, S. Mochizuki, S. Sakaino, Y. Kaneko, S. Abe, and S. Abe, "Bidirectional contactless power transfer system expandable from unidirectional system,"in *Proc. Energy Convers. Congr. Expo.*, 2013, pp. 3651–3657.

[12] T. Imura and Y. Hori, "Maximizing air gap and efficiency of magnetic resonant coupling for wireless power transfer using equivalent circuit and Neumann formula," *IEEE Trans. Ind. Electron.*, vol. 58, no. 10, pp. 4746–4752, Oct. 2011.

[13] W. Zhang, S. C. Wong, C. K. Tse, and Q. Chen, "Design for efficiency optimization and voltage controllability of series-series compensated in-

ductive power transfer systems," *IEEE Trans. Power Electron.*, vol. 29, no. 1, pp. 191–200, Jan. 2014.
[14] S. Y. Cho, I. O. Lee, S. C. Moon, B. C. Kim, and K. Y. Kim, "Series-series compensated wireless power transfer at two different resonant frequencies," in *Proc. ECCE Asia Downunder*, 2013, pp. 1052–1058.
[15] C. Duan, C. Jiang, A. Tayllor, and K. Bai, "Design of a zero-voltage-switching large-air-gap wireless charger with low electric stress for electric vehicles," *IET Power Electron.*, vol. 6, no. 9, pp. 1742–1750, 2013.
[16] B. Wang, A. P. Hu, and D. Budgett, "Maintaining middle zero voltage switching operation of parallel-parallel tuned wireless power transfer system under bifurcation," *IET Power Electron.*, vol. 7, no. 1, pp. 78–84, 2014.
[17] D. J. Thrimawithana, U. K. Madawala, and Y. Shi, "Design of a bi-directional inverter for a wireless V2G system," in *Proc. IEEE Int. Conf. Sustainable Energy Technol.*, 2010, pp. 1–5.
[18] C. Tang, X. Dai, Z. Wang, Y. Su, and Y. Sun, "A bidirectional contactless power transfer system with dual-side power flow control," in *Proc. IEEE Int. Conf. Power Syst. Technol.*, 2012, pp. 1–6.
[19] D. J. Thrimawithana, U. K. Madawala, and M. Neath, "A steady-state analysis of bi-directional inductive power transfer systems," in *Proc. IEEE Int. Conf. Ind. Technol.*, 2013, pp. 1618–1623.
[20] H. Kudo, K. Ogawa, N. Oodachi, N. Deguchi, and H. Shoki, "Detection of a metal obstacle in wireless power transfer via magnetic resonance," in *Proc. IEEE Telecommun. Energy Conf.*, 2011, pp. 1–6.
[21] H. Kikuchi, "Metal-loop effects in wireless power transfer systems analyzed by simulation and theory," in *Proc. IEEE Electr. Design Adv. Packag. Syst. Symp.*, 2013, pp. 201–204.
[22] J. G. Bolger, F. A. Kirsten, and L. S. Ng, "Inductive power coupling for an electric highway system," in *Proc. IEEE 28th Veh. Technol. Conf.*, 1978, pp. 137–144.
[23] G. A. J. Elliott, J. T. Boys, and A. W. Green, "Magnetically coupled systems for power transfer to electric vehicles," *Power Electron. Drive Syst.*, vol. 2, pp. 797–801, 1995.
[24] T. Imura, H. Okabe, and Y. Hori, "Basic experimental study on helical antennas of wireless power transfer for electric vehicles by using magnetic resonant couplings," in *Proc. IEEE Vehicle Power Propulsion Conf.*, 2009, pp. 936–940.
[25] Y. Nagatsuka, N. Ehara, Y. Kaneko, S. Abe, and T. Yasuda, "Compact contactless power transfer system for electric vehicles," in *Proc. Int. Power Electron. Conf.*, 2010, pp. 807–813.
[26] S. Li and C. C. Mi, "Wireless power transfer for electric vehicle applications," in *Proc. Emerg. Sel. Topics Power Electron.*, 2014, pp. 1–14.
[27] H. Fujimoto, T. Miyajima, J. Amada, "Development of electric vehicle with variable drive unit system," presented at the Int. Electric Vehicle Technology Conf. Japan, (EVTEC), 2014.
[28] SAE International. (2013). Wireless charging advances with selection of 85-kHz charging frequency. [Online]. Available: http://articles.sae.org/12647/.
[29] M. Kato, T. Imura, and Y. Hori, "New characteristics analysis considering transmission distance and load variation in wireless power transfer via magnetic resonant coupling," in *Proc. Intelec*, 2012, pp. 1–5.

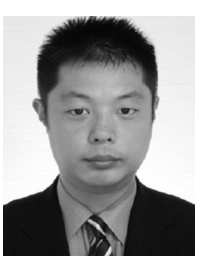

Motoki Sato (M'12) received the M.E. degree from the Nagaoka University of Technology, Nagaoka, Japan, in 2005. He is currently working toward the Ph.D. degree in the Graduate School of Frontier Sciences, The University of Tokyo, Chiba, Japan.

He joined Toyo Denki Seizo K.K., Kanagawa, Japan, in 2005. His research interests include wireless power transfer and power electronics.

Mr. Sato is a member of the Institute of Electrical Engineers of Japan.

Gaku Yamamoto received the B.S. degree from the Tokyo University of Science, Tokyo, Japan, in 2013 and the M.S degrees from The University of Tokyo, Japan, in 2015.

He is currently with Nissan Motor Co., Ltd., Kanagawa, Japan.

Mr. Yamamoto is a member of the Institute of Electrical Engineers of Japan.

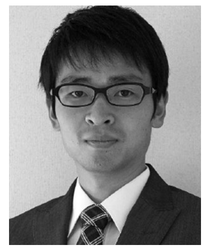

Daisuke Gunji (M'13) received the B.S. and M.S. degrees in mechanical engineering and intelligent systems from The University of Electro-Communications, Tokyo, Japan, in 2005 and 2007, respectively and the Ph.D. degree from the Graduate School of Frontier Sciences, The University of Tokyo, Chiba, Japan, in 2015.

In 2007, he joined NSK, Ltd,, Kanagawa, Japan. His research interests include wireless power transfer, motion control, and electric vehicle control.

Dr. Gunji is a member of the Institute of Electrical Engineers of Japan, the Society of Automotive Engineers of Japan, the Japan Society of Mechanical Engineers, and the Robotics Society of Japan.

Takehiro Imura (S'09–M'10) received the bachelors degree in electrical and electronics engineering from Sophia University, Tokyo, Japan, in 2005, and the M.E. degree in electronic engineering and the D.Eng. degree in electrical engineering from The University of Tokyo, Tokyo, in 2007 and 2010, respectively,

He joined the Department of Advanced Energy, Graduate School of Frontier Sciences, The University of Tokyo, as a Research Associate, where since 2015, he has been a Project Lecturer. He is currently investigating wireless power transfer for EV using electromagnetic resonance coupling.

Hiroshi Fujimoto (S'99–M'01–SM'13) received the Ph.D. degree from the Department of Electrical Engineering, University of Tokyo, Tokyo, Japan, in 2001.

In 2001, he joined the Department of Electrical Engineering, Nagaoka University of Technology, Nagaoka, Japan, as a Research Associate. From 2002 to 2003, he was a Visiting Scholar in the School of Mechanical Engineering, Purdue University, West Lafayette, IN, USA. In 2004, he joined the Department of Electrical and Computer Engineering, Yokohama National University, Yokohama, Japan, as a Lecturer and became an Associate Professor in 2005. He has been an Associate Professor with the University of Tokyo, since 2010.

Dr. Fujimoto received the Best Paper Award from the IEEE TRANSACTIONS ON INDUSTRIAL ELECTRONICS in 2001. His research interests include control engineering, motion control, nanoscale servo systems, electric vehicle control, and motor drive.

Dr. Fujimoto is a member of the IEE of Japan, the Society of Instrument and Control Engineers, the Robotics Society of Japan, and the Society of Automotive Engineers of Japan.